Int. J. Electrochem. Sci., 14 **(2019)** 11092 – 11101, doi: 10.20964/2019.12.11

International Journal of
ELECTROCHEMICAL
SCIENCE
www.electrochemsci.org

Short Communication

Study on Preparation and Properties of Tungsten Coating Based on WC Electrolysis

Qinghua Zhang[1,2], *Xiaoli Xi*[1,2,*], *Wenxuan Qin*[1], *Liwen Zhang*[1], *Liwen Ma*[2], *Zuoren Nie*[1,2]

[1] National Engineering Laboratory for Industrial Big-data Application Technology, Beijing University of Technology, Beijing 100124, China
[2] College of Materials Science and Engineering, Key Laboratory of Advanced Functional Materials, Education Ministry of China, Beijing University of Technology, Beijing 100124, China
[*]E-mail: zhangqinghua@emails.bjut.edu.cn, xixiaoli@bjut.edu.cn

Received: 16 July 2019 / *Accepted:* 7 September 2019 / *Published:* 29 October 2019

Tungsten carbide (WC) is used as an anode in molten sodium tungstate to prepare a tungsten coating. Recovery of tungsten powder from WC electrolysis has been extensively studied, but the possibility of making available Tungsten coatings is still unrealized. A theoretical analysis was first carried out, and the feasibility of electrolysis was confirmed. Subsequently, this conclusion was also verified experimentally. In this experiment, the coating was studied by regulating the cathode current density. The tungsten coatings prepared at various current densities were characterized by X-ray Diffraction (XRD), Scanning Electron Microscope-Energy Dispersive Spectroscopy (SEM-EDS), nanoindentation tests, and Laser Scanning Confocal Microscopy LSCM. The results show that at a cathode current density of 70 $mA \cdot cm^{-2}$, an optimized tungsten coating can be obtained. The tungsten coating has a thickness of 4.1 μm and a minimum average grain size.

Keywords: Molten salt, tungsten coating, tungsten carbide recovery

1. INTRODUCTION

Tungsten is a refractory metal with the highest melting point as well as excellent physical and chemical properties, high strength, and hardness. The alloys and compounds of tungsten are widely used, and the popular products are tungsten electrode, tungsten filament, high-temperature alloy, and cemented carbide, which is the most widely used tungsten product. Cemented carbide is known as “industrial teeth” because it is the most widely used tool material in the industry. 54% of the world’s tungsten resources are used to produce cemented carbide products; this ratio is even as high as 66% in the United States [1–4]. However, the tungsten reserves in the world are decreasing year by year. Because of current industrial expansion, the consumption of tungsten products is rapidly rising. The tungsten content in waste cemented carbide is as high as 74–99%, whereas the tungsten content in the ore is only 0.06–1.2%. Therefore, to avoid the depletion of resources, it is necessary to utilize the secondary resources of tungsten in industrial practice [5]. The recovery methods for traditional cemented carbides mainly include crushing, zinc melting, and oxidation, but they suffer from long and cumbersome processes [6,7]. In contrast, molten salt electrolysis has great advantages in these respects [8–12].

As mentioned above, tungsten has excellent physical and chemical properties, but its difficult processing characteristics limit its application. The use of tungsten as a coating material to improve the performance of matrix material has attracted much attention [13].

Important processing methods for tungsten coating are plasma spraying [14], physical vapor deposition [15], vapor deposition [16], and molten salt electrodeposition. In an aqueous solution, tungsten cannot be electrodeposited alone; tungsten can only be co-deposited with iron-based metals in the form of alloys [17]. A pure tungsten coating must exist in the molten salt medium, and the tungsten coating can be prepared using the molten salt plating method by one-step electrolysis. Impurities such as oxygen can be avoided, and the method and process can be easily controlled [18].

Therefore, it is essential to recover and process tungsten by molten salt electrolysis. Recovery of tungsten carbide (WC) usually involves the preparation of a powder, and the powder is subjected to subsequent processing to obtain a tungsten product. For example, molten salt electrolysis recovers a cemented carbide to obtain a metal tungsten powder, and then the tungsten powder is subjected to plasma spraying to prepare a tungsten coating. This process is time-consuming and laborious.

In some studies, tungsten coatings have been prepared from a molten salt. Zhang et al. obtained a pure tungsten coating in Na_2WO_4-WO_3, where sodium tungstate acts as a solvent and tungsten trioxide acts as a solute and provides a tungsten source [19–22]. In this paper, to achieve efficient remanufacturing of tungsten, tungsten coatings were obtained from molten sodium tungstate using WC as a consumable anode. The preparation and structural properties of tungsten coatings at various cathode current densities were studied. The effect of various current densities on the characteristics of tungsten coatings was evaluated.

2. EXPERIMENTAL

All chemical reagents are of analytical grade. In experiments, sodium tungstate was utilized as a molten salt electrolyte. WC (99.95%) was wire cut into blocks with a size of 3×3×20 mm^3 and used as an anode. A molybdenum plate (99.95%) with a size of 1×6×10 mm^3 was used as the cathode. In this study, WC was used as the anode, and the tungsten layer was electrocoated on the cathode by molten salt electrolysis. The electrodes were prepolished and then cleaned by ultrasonication in deionized water, ethanol, and acetone in turn. The experimental procedure can be described as follows: The molten salts were predried for 24 h, taken out during the experiment, and then placed in the reactor. After the electrodes were assembled, the electrolytic furnace was sealed. Then, the furnace was maintained in a vacuum state, and the temperature was maintained at 300 ℃ for 2 h. A schematic diagram of the electrolytic reactor is shown in Fig. 1 (a). It was made of high-purity aluminum trioxide (99.5%) and placed on a support table in the furnace. Then, argon gas was passed into the furnace and maintained in connection with the atmosphere. The temperature of furnace was increased to 900 ℃.

This temperature was maintained for another 2 h to completely dissolve the molten salt. Then, the system was available for experiment. The electrodes needed in the experiment were immersed in molten salt, and a multimeter was used to determine whether the electrodes were connected or not. The immersion depth was precisely controlled. At the same time, an electrochemical workstation was connected, and the specified parameters were set for electrolysis. All electrochemical measurements were carried out using a PARSTAT 4000 electrochemical working station along with a Versa Studio software package (Advanced Measurement Technology, Inc., USA). The working and reference electrodes are both platinum wires (99.99%, 0.5 mm diameter), and the auxiliary electrode is graphite (2.0 mm diameter). Electrochemical behavior was studied by cyclic voltammetry (CV) and chronoamperometry (CA). The coatings were characterized by scanning electron microscopy (SEM, JSM-7001F, EDS, Pegasus XM2), X-ray diffraction (XRD, Bruker, AdvanceD-8X, Cu Kα 1 radiation, 2°/min) analyses, nanoindentation tests, and laser scanning confocal microscopy (LSCM). The grain size was calculated by taking five SEM images of different positions of the same coating, counting by Image J, and taking the average.

3. RESULTS AND DISCUSSION

3.1 Feasibility study

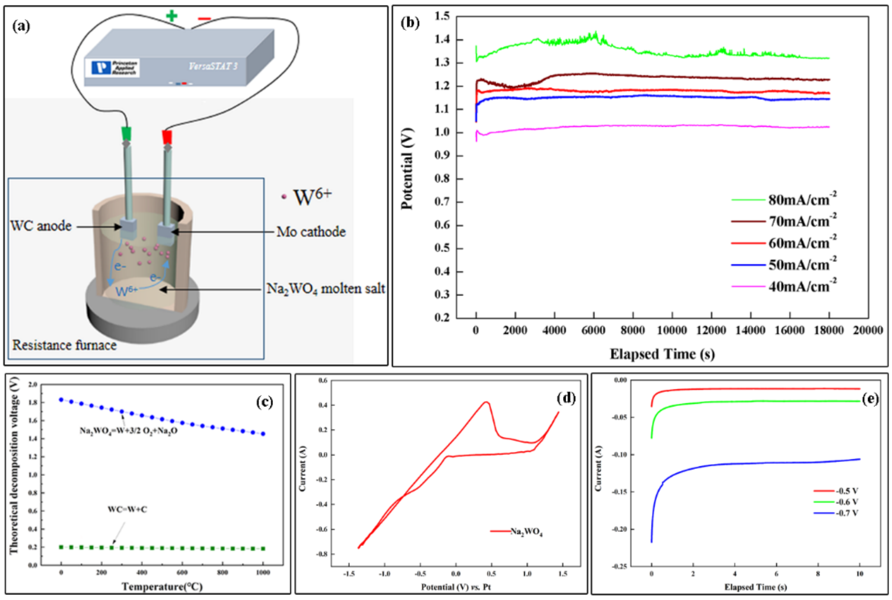

Figure 1. (a) Reaction device diagram, (b) cell voltage–time curve (900 °C) (c) theoretical decomposition voltage diagram, (d) CV curve (900 °C; scan rate:100 mv/s; scan range: –1.5 V to 1.5 V), (e) chronoamperometric curve (900 °C)

The theoretical decomposition voltage of the two electrode reactions was calculated using thermodynamic calculation software HSC 6.0, as shown in Fig. 1 (c). In the experimental temperature range, the WC decomposition voltage is always lower than the theoretical decomposition voltage of sodium tungstate. This verifies the feasibility of electrochemical dissolution of WC in sodium tungstate. When the electrolysis temperature reaches 900 °C, to avoid the decomposition of sodium tungstate and ensure a stable progress of electroplating, the voltage should be controlled between 0.18 V and 1.48 V. Fig. 1(b) shows that the actual cell voltage at various cathode current densities is between 1.0 V and 1.4 V. Therefore, the decomposition of molten salt should not occur during this process, and the molten salt electrolysis can be stably performed. Fig. 1(d) shows the CV curves of molten sodium tungstate, indicating a distinct oxidation peak (0.37 V) and a reduction peak (from about −0.5 V to −0.7 V) corresponding to the oxidation and reduction of tungsten, respectively. However, the reduction peak is not obvious, and the reduction potential is not clear. To further determine the reduction potential, CA was carried out, as shown in Fig. 1(e). A large current change occurs between −0.6 V and −0.7 V, indicating that the position of reduction peak is between −0.6 V and −0.7 V. The preparation of coating is focused on the reduction of tungsten by cathodic reaction, i.e., the cathode potential should be negative than −0.7 V in actual experiments.

3.2 Surface composition and morphology

Electroplating was carried out for 5 h at 900 ℃ using WC as the anode, and the cathode current densities were set as 40 mA·cm^{-2}, 50 mA·cm^{-2}, 60 mA·cm^{-2}, 70 mA·cm^{-2}, and 80 mA·cm^{-2}. The XRD results of the coating are shown in Fig. 2. The current density significantly affects the phase of coating. The cathode product obtained at 40 mA·cm^{-2} is mainly W_2C phase.

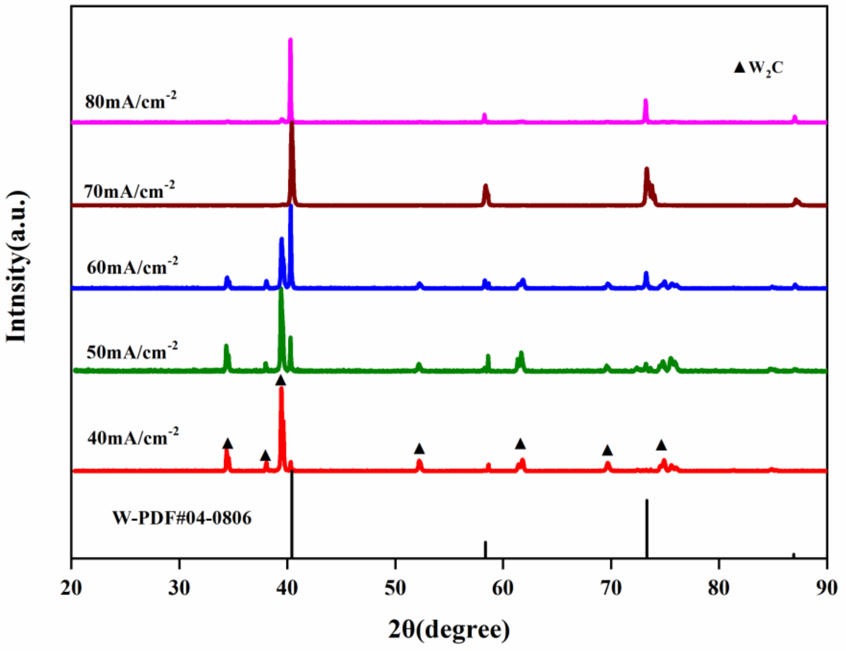

Figure 2. XRD pattern of coatings

As the current density increases, the phase gradually evolves and finally transforms into W phase. This is probably because at a high cathode current density, the cathode tungsten ions are electrically reduced faster, and the migration rate of carbon atoms is constant. Therefore, the proportion of W_2C involved in the reaction is higher. At low current densities, the presence of W_2C adversely affects the uniform distribution of coating, consistent with the SEM results. From the phase perspective, 70 mA·cm^{-2} and 80 mA·cm^{-2} were considered as the more optimized conditions. When tungsten was used as the anode, in Na_2WO_4-WO_3 system, the phases of all coatings were tungsten, and no W_2C existed [20–22]. This indicates that the carbon atom of W_2C originates from the anode. Therefore, to obtain the coating with a single tungsten phase using this method, the cathode current density is a crucial parameter.

Fig. 3 shows the surface morphology of coating. The surface of coating is smooth and dense without obvious macroscopic defects. This indicates that the electrolysis was smoothly carried out.

In addition, the vignettes in Fig. 3 show the high-magnification SEM images of coatings. At a current density of 40 mA·cm^{-2}, the coating has not yet formed a uniform microscopic morphology, and the grain stacking is not uniform. This may be caused by two reasons. First, the crystal nucleation rate is low, resulting in less grain per unit area. Second, the presence of an impurity phase adversely affects the uniform distribution. At 50 mA·cm^{-2}, the grain filling is more compact. At 60 mA·cm^{-2}, the individual crystal grains are more densely arranged and substantially free of pores. When the current density is 70 mA·cm^{-2}, owing to the high current density, the grain is refined and compact. The deposition of a single phase promotes uniform alignment of grains. No pores exist, but in some cases, nodules occur. When the current density reached 80 mA·cm^{-2}, large crystal nodules appeared in the grains. In Fig. 4, the grain has a minimum at 70 mA·cm^{-2}.

3.3 Characterization of coating surface properties

3.3.1 Roughness test:

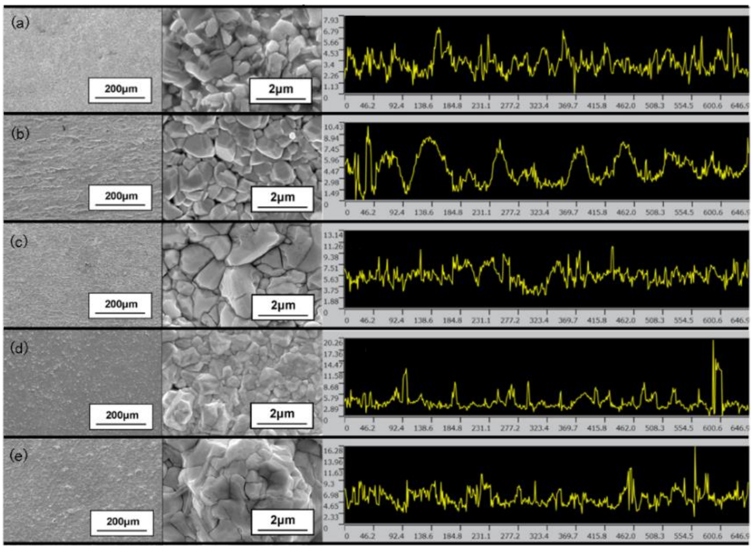

Figure 3. SEM images and linear profiles test of the coating surface. (a) 40 mA·cm^{-2}, (b) 50 mA·cm^{-2}, (c) 60 mA·cm^{-2}, (d) 70 mA·cm^{-2}, (e) 80 mA·cm^{-2}

The right side of Fig. 3 shows a linear profiles test of the coatings at various current densities. As the current density increases, the surface roughness shows an increasing trend. At higher current densities, the surface of coating has nodules, and the surface undulation is large. Protrusions appearing in the profile can be reflected by the line of nodulation. In general, the content shown on the SEM images is consistent with the linear profiles test.

Electrochemical polarization significantly affects crystallization [23–25]. When electrochemical polarization occurs, a Tafel relationship exists between the electrochemical overpotential and current density: As the current density increases, the electrochemical polarization increases. Electromorphic nucleation and growth rate can be expressed by the following formulas when the coating is deposited:

$$\text{Nucleation rate: } V_1 = K_1 e^{-\eta^{-2}}$$

$$\text{Growth rate: } V_2 = K_2 e^{-\eta^{-1}}$$

where V_1 is the crystal nucleation rate; V_2 is the crystal growth rate; η is the electrochemical polarization overpotential; K_1 and K_2 are all constant.

With the increase in current density, the electrochemical polarization increases, the crystal nucleation rate of coating increases faster than the crystal growth rate, and the grains get refined. This is consistent with the uniformity of surface morphology. This is shown by a decrease in surface roughness.

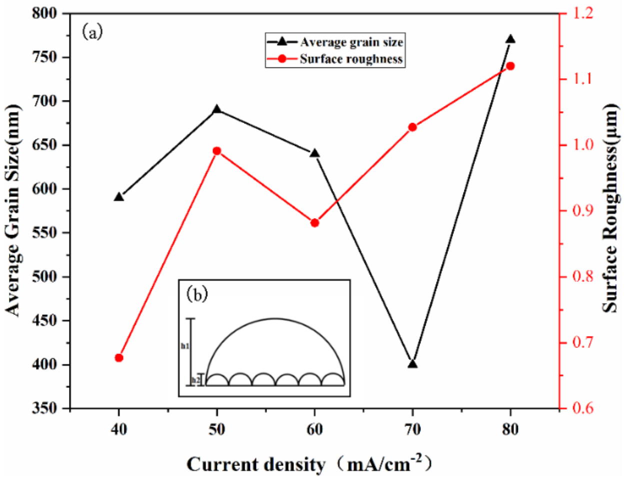

Figure 4. (a) Effect of current density on grain size and roughness of coating. (b) Relationship between grain size and surface roughness under ideal conditions

The average grain size and roughness of coatings at different cathode current densities are shown in Fig. 4(a). When 70 mA·cm^{-2} was excluded, the average grain size and roughness have a consistent trend. A theoretical model is presented in Fig. 4(b). Assuming that the grains are uniform spheres, as the grain size increases, larger grains have a larger radial fluctuation range per unit length. This reflection on the surface represents a greater roughness. In practice, the shape of the grains is more complicated, as shown in Fig. 3. Most of the grains are irregular polyhedra, which may deviate from our theoretical model. But overall, this ideal model proves to be reasonable and is beneficial for understanding the relationship between grain size and roughness.

The decrease in average grain size at 50–70 mA·cm^{-2} can be attributed to the increase in electrochemical polarization. A finer grain corresponds to better surface uniformity, resulting in a smaller surface roughness. The inconsistency in the 70 mA ·cm^{-2} trend is probably because the coating begins to form nodules in this case, thus increasing the roughness. At 80 mA·cm^{-2}, the grain size increases abnormally, probably because the cluster growth of crystal grains consumes a large overpotential, decreasing the nucleation overpotential.

3.3.2 Nanoindentation test

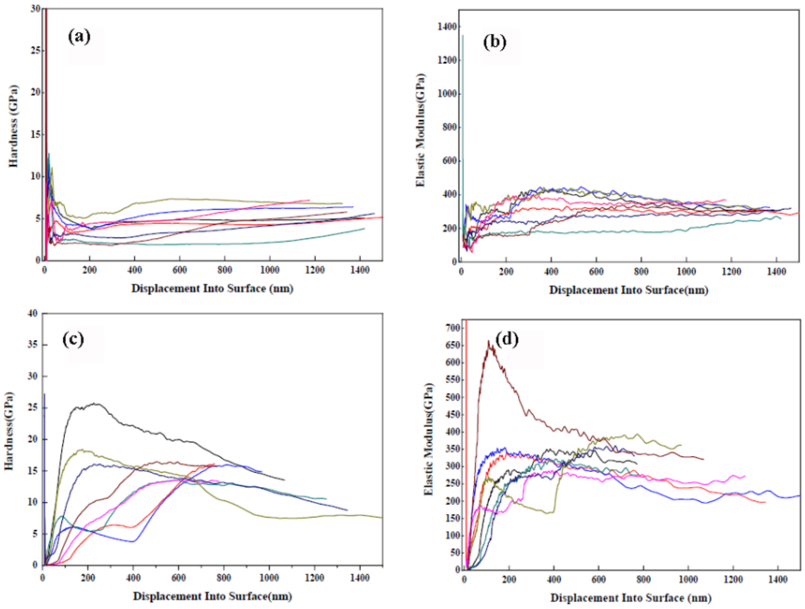

Figure 5. (a) Relationship between indentation depth and hardness of sample 1. (b) Relationship between indentation depth and elastic modulus of sample 1. (c) Relationship between indentation depth and hardness of sample 2. (d) Relationship between indentation depth and elastic modulus of sample 2.

Nanoindentation tests were performed on two samples, each taking 10 points, and the curves between indentation depths and hardness (or elastic modulus) are shown in Fig. 5. Samples 1 and 2 were prepared under conditions of 70 and 50 mA·cm^{-2}, respectively. According to Section 3.2, the XRD results of Sample 1 show that the main phase is W. The XRD results of Sample 2 show that the main phase is W_2C, and a part of W phase is present. The test data show that the hardness of Sample 1 is 6.01 GPa, close to that reported in the literature [26]. The modulus of elasticity is 331.0 GPa, close to the elastic modulus of tungsten of 344.7 GPa. The tungsten coating has properties comparable to those of as-sintered tungsten block. Sample 2 has a hardness of 13.11 GPa and an elastic modulus of 288.3 GPa. The hardness of Sample 2 is much larger than that of Sample 1. This is closely related to the W_2C hard-phase distribution in the coating. Although Sample 2 has excellent hardness, it suffers from performance inhomogeneity and reliability for industrial applications. In contrast, coatings with a single tungsten phase do not have such problems. Therefore, sample 1 was considered as the more optimized product.

3.3.3 Cross-section test and component analysis

On the basis of the above analysis, the most favorable cathode current density of W coating is 70 mA·cm^{-2}. The coating obtained under this condition was further characterized by thickness and composition. Sample 1 was subjected to cold setting treatment, and the cross-section was observed under a scanning electron microscope, as shown in Fig. 6 (a). A clearly distinguishable two-layer substance was observed in the secondary electron mode. Line scanning analysis of the cross-section of coating/substrate interface proves that the substrate was molybdenum, and the coating was tungsten. Moreover, tungsten is interstitially grown at the voids on the surface of molybdenum substrate, and after filling the voids, the tungsten gradually extends and becomes thick. The line scanning analysis of cross-section of tungsten coating shows that the tungsten and molybdenum layers are present on both sides. The thickness of position in Fig. 6 was measured to be about 4.1 microns. The coating composition under this condition was further analyzed. Fig. 6 (b) shows the XPS analysis of W4F core layer: The $4f_{5/2}$ and $4f_{7/2}$ peaks of W appear, and the corresponding binding energies are 33.2 eV and 31.0 eV, respectively [27]. These two peaks are formed by zero-valent tungsten, further indicating that the coating is composed of metallic tungsten.

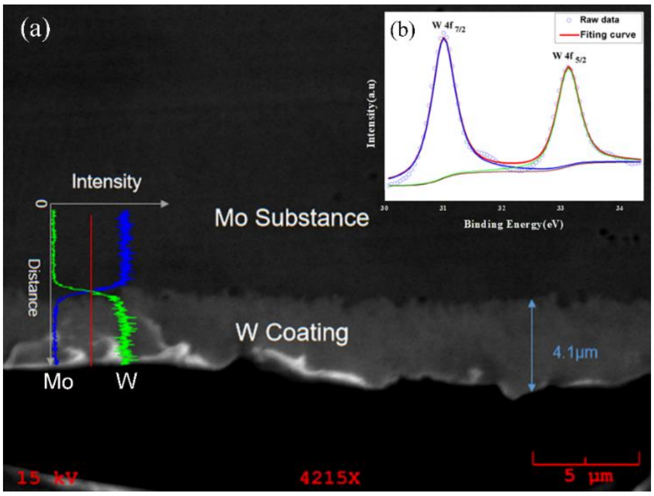

Figure 6. (a) Sectional view of Sample 1. (b) XPS analysis of Sample 1.

4. CONCLUSION

In this study, the theoretical decompositions of sodium tungstate and WC were first calculated using thermodynamic calculation software HSC, indicating the theoretical feasibility of electrolytic WC in molten sodium tungstate. Subsequently, the feasibility of actual electrolysis was verified from the cell voltage–time curve of electrolysis. Electrochemical testing showed the potential of redox peak of tungsten. The increase in cathode current density significantly affects the product phase, and the coating undergoes a transition of the main phase from W_2C phase to W phase. The macrosurface of coating is dense and void-free. As the current density increases, the microscopic appearance involves the gradual solidification of grains, and nodule phenomenon occurs when the current density is too large. The roughness of tungsten coating at different current densities has a corresponding relationship with the grain size. The optimum condition was 70 mA·cm^{-2}: The coating is mainly composed of tungsten and has the smallest grain size. The hardness of coating is 6.01 GPa, and the modulus of elasticity is 331.0 GPa. The thickness of coating is ~4.1 μm.

ACKNOWLEDGEMENTS
This work was supported by National Natural Science Foundation of China (51621003), Beijing Municipal Natural Science Foundation (2172010) and the Fundamental Research Funds for Science and Technology Innovation Service Capacity-building (Beijing municipal level PXM2019_014204_500032).

References

1. D.R. Leal-Ayala, J.M. Allwood, E. Petavratzi, T.J. Brown and G.Gunn, *Resour., Conserv. Recycl.,* 103 (2015) 19.
2. E. Lassner, W.-D. Schubert, *Springer Science & Business Media*, (1999) 124.
3. A. Koutsospyros, W. Braida, C. Christodoulatos, D. Dermatas and N. Strigul, *J. Hazard. Mater.,* 136 (2006) 19.
4. W.G. Jung, *J. Ind. Eng. Chem.,* 20 (2014) 2384.
5. A. Shemi, A. Magumise, S. Ndlovu and N. Sacks, *Miner. Eng.,* 122 (2018) 195.
6. L. Luo, L.K. Jun, A. Shibayama, W.T. Yen, T. Fujitac, O. Shindod and A. Kataid, *Hydrometallurgy,* 72 (2004) 1.
7. B. Liu, A. Shi, G. Yang, Q. Su, G. Chen, L. Zhang and B. Yang, *Int. J. Refract. Met. Hard Mater.,* 67 (2017) 74.
8. X.L. Xi, G.H. Si, Z.R. Nie and L.W. Ma, *Electrochim. Acta,* 184 (2015) 233.
9. X.L. Xi, X.J. Xiao, Z.R. Nie, L.W. Zhang and L.W. Ma, *J. Electroanal. Chem.,* 794 (2017) 254.
10. X.J. Xiao, X.L. Xi, Z.R. Nie, L.W. Zhang and L.W. Ma, *Metall. Mater. Trans. B,* 48 (2017) 692.
11. L.W. Zhang, Z.R. Nie, X.L. Xi, L.W. Ma, X.J. Xiao and M. Li, *Metall. Mater. Trans. B,* 49 (2018) 334.
12. G.H. Si, X.L. Xi, Z.R. Nie, L.W. Zhang and L.W. Ma, *Int. J. Refract. Met. Hard Mater.,* 54 (2016) 422.
13. F. Jiang, Y.C. Zhang, N.B. Sun and Z.A. Liu, *Appl. Surf. Sci.,* 317 (2014) 867.
14. Y. Yahiro, M. Mitsuhara, K. Tokunakga and N. Yoshida, T. Hirai, K. Ezato, S. Suzuki, M. Akiba and H. Nakashima, *J. Nucl. Mater.,* 784 (2009) 386.
15. C. Ruset, E. Grigore, H. Maier, R. Neu, H. Greuner, M. Mayer and G. Matthews, *Fusion Eng. Des.,* 86 (2011) 1677.
16. J.H. Du, Z.X. Li, G.J. Liu, H. Zhou and C.L. Huang, *Surf. Coat. Technol.,* 198 (2005) 169.
17. A. Bodaghi, J. Hosseini, *Int. J. Electrochem. Sci.,* 7 (2012) 2584.
18. Y.F. Qi, Y.H. Tang, B. Wang, M. Zhang, X.Q. Ren, Y.G. Li and Y.T. Ma, *Int. J. Refract. Met. Hard Mater.,* 81 (2019) 183.
19. H.S. Zhou, Y.P. Xu, N.B. Sun and Y.C. Zhang, Y. Oya, M.Z. Zhao, H.M. Mao, F. Ding, F. Liu, G.N. Luo and EAST Contributors, *Fusion Eng. Des.,* 113 (2016) 265.
20. N.B. Sun, Y.C. Zhang, F. Jiang, S.T. Lang and M. Xia, *Fusion Eng. Des.,* 89 (2014) 2529.
21. F. Jiang, Y.C. Zhang, X.L Li, N.B. Sun and L.L. Wang, *Fusion Eng. Des.,* 89 (2014) 83.
22. F. Jiang, Y.C. Zhang, N.B. Sun and J.X. Leng, *Appl. Surf. Sci.,* 327 (2015) 432.
23. R. Winand, *J. Appl. Electrochem.,* 21 (1991) 377.
24. A. Weymeersch, L. Renard, *Plat. Surf. Finish.,* 6 (1986) 68.
25. L.A. Zhu, S.X. Bai, H. Zhang and Y.C. Ye, *Appl. Surf. Sci.,* 265 (2013) 537.

26. W. Zhang, X.Q. Gao, P.X. Zhang, Z.W. Hu, L.P. Li and J. Cheng, *Rare Metal Mat. Eng.,* 46 (2017) 3626.
27. W. Chen, J.T. Roberts, *Surf. Sci.,* 324 (1995) 169.